
Huff-LLM: End-to-End Lossless Compression for Efficient LLM Inference

Patrick Yubeaton^{*1} Tareq Mahmoud^{*2} Shehab Naga^{*2} Pooria Taheri^{*2} Tianhua Xia^{*1} Arun George²
 Yasmein Khalil² Sai Qian Zhang¹ Siddharth Joshi² Chinmay Hegde¹ Siddharth Garg¹

Abstract

As they become more capable, large language models (LLMs) have continued to rapidly increase in size. This has exacerbated the difficulty in running state of the art LLMs on small, edge devices. Standard techniques advocate solving this problem through lossy compression techniques such as quantization or pruning. However, such compression techniques are lossy, and have been shown to change model behavior in unpredictable manners. We propose Huff-LLM, an *end-to-end, lossless* model compression method that lets users store LLM weights in compressed format *everywhere*—cloud, disk, main memory, and even in on-chip memory/buffers. This allows us to not only load larger models in main memory, but also reduces bandwidth required to load weights on chip, and makes more efficient use of on-chip weight buffers. In addition to the memory savings achieved via compression, we also show latency and energy efficiency improvements when performing inference with the compressed model.

1. Introduction

State-of-art Large language models (LLMs) are *massive*—even a mid-size model like Llama3-70B (Dubey et al., 2024) takes up 150GB of memory, which is out of reach except for the highest-end hardware. Model size not only limits deployment on edge devices that tend to have small memory capacity, but also increases the memory bandwidth required for fast inference. Massive model sizes have motivated a large body of work on model compression targeted specifically for LLMs. These methods primarily fall into two buckets: quantization and pruning. Quantization methods seek to decrease the precision of model parameters, thus requiring fewer bits per parameter, while pruning methods

seek to decrease the number of parameters. Recent works such as LLM.Int8() (Dettmers et al., 2022), GPTQ (Frantar et al., 2022), and AWQ (Lin et al., 2024) have achieved $2\times-4\times$ compression with respect to LLM weights, thereby potentially speeding up inference.

However, quantization and pruning are both lossy compression methods, leading the compressed models to behave differently from the original model and flipping incorrect to correct answers (and vice versa) on multiple-choice benchmarks even if average accuracy is maintained (Dutta et al., 2024). Safety, trustworthiness, multilingual capabilities and demographic biases might also be impacted, as shown by (Xu et al., 2024; Hong et al., 2024; Marchisio et al., 2024). These results demonstrate that, notwithstanding the impressive results obtained from lossy model compression, we have yet to fully understand its impact on LLM behaviour. This raises the question: *can we compress LLMs without altering their behaviour in any way?*

Lossless compression methods (such as Huffman coding and arithmetic coding) offer a solution. Just as how a Huffman-compressed image can be reconstructed exactly in its original form; a losslessly compressed LLM model would behave *identically* to the original model after decompression. However, despite widespread use in other domains, lossless compression has found surprisingly little application in LLM compression. One main reason is that lossless compression and decompression can be *computationally expensive* and is not natively supported on commodity hardware like CPUs and GPUs. Custom hardware accelerators (such as TPUs and NPUs) also do not implement lossless compression due to hardware implementation overheads.

Prior work has proposed lossless compression to reduce download costs of LLM weights from the cloud (Hershcovitch et al., 2024), but the model is decompressed and loaded into memory in its original, uncompressed format. (Hao et al., 2024) go a step further: models are loaded into memory in compressed form, but decompressed layer by layer during inference. Thus, larger models can be loaded into a smaller main memory, but at the cost of *increased* inference latency since weight matrices must first be decompressed before inference. As a result, prior methods do not realize the *full* benefits of model compression, including reduced

^{*}Equal contribution ¹Department of Electrical and Computer Engineering, New York University, NY, USA ²Department of Computer Science and Engineering, University of Notre Dame, IN, USA. Correspondence to: Patrick Yubeaton <wp2004@nyu.edu>.

download costs and memory footprint, but also faster and more energy-efficient LLM inference.

Our contributions. We propose HUFF-LLM, a new *end-to-end* model compression method and custom hardware implementation that stores LLM weights in compressed format *everywhere*—cloud, disk, main memory, *and* in on-chip memory/buffers. Weights are only decompressed when needed, *i.e.*, to multiply with inputs/activations, where they are decompressed to their original FP16/BF16 formats. Via careful hardware-software co-design, we ensure that HUFF-LLM is both lightweight, adding less than 6% area overhead, and easily integrated into custom hardware architectures like systolic arrays and vector-accelerator (Sijstermans, 2018; Shao et al., 2019; Keller et al., 2022) architectures commonly used in today’s TPU/NPU chips. Using simulations and an FPGA prototype, we show that HUFF-LLM reduces model size by up to 32%, improves inference latency by up to 31%, *and* cuts energy cost by up to 26%. Our main contributions are as follows:

- We introduce HUFF-LLM, an end-to-end model compression technique which is capable of maintaining LLM weights in compressed format throughout the system when using custom hardware.
 - Rather than applying Huffman compression to the whole parameter, HUFF-LLM compresses subsets of LLM weight parameters. This minimizes the overheads of Huffman decompression, rendering it practical.
 - We develop a Huffman decoder that can, with minimal overhead, be integrated into standard accelerator architectures like Systolic Arrays and Vector Processors.
- Our evaluations across multiple LLM architectures demonstrate that HUFF-LLM achieves a 15–32% reduction in both required on-chip memory capacity and memory bandwidth requirements.
- We evaluate HUFF-LLM’s compression performance using accelerator design tools, simulations, and standard performance estimators across multiple accelerator architectures and popular open-weight LLM families.
 - We observe consistent savings across architectures, with up to 31% improvement to latency and up to 26% reduction in energy.

2. Background and Related Work

2.1. LLM Model Compression

LLM Weight Formats. LLM weights are broadly stored in either floating point or integer formats during inference. The most common floating point formats are 32-bit floating point (FP32), 16-bit floating point (FP16), and 16-bit brain

float (BF16). In FP16, for instance, the most significant bit (MSB) is the sign (S) of the number, the next five bits are the exponent (E), and the last ten bits are the mantissa (M). Any FP16 weight is then represented as:

$$\text{Value} = (-1)^S \times 2^{E-B} \times (1.M) \quad (1)$$

where B is a fixed bias term, commonly set to $B = 15$. In this format, mantissa bits only encode the fractional value after the decimal point ($1.M$). FP32 is similar, but allocates 8 bits to the exponent and 23 bits to the mantissa. BF16, introduced as a compromise between FP32 and FP16, has an 8-bit exponent, a 7-bit mantissa, and a sign bit. BF16 has a larger dynamic range compared to FP16, but lower precision within this range compared to FP16.

To reduce model size, 8-bit integer (INT8) and 4-bit integer (INT4) formats were introduced. These represent weights as signed 2’s-complement integers. Decimals are represented using a scaling factor typically associated with an entire tensor or channels within it. INT8 and INT4 representations are typically obtained via quantization methods applied to models stored in FP16 or BF16 formats. These methods are discussed next.

LLM Weight Quantization As LLM sizes have grown, their associated workloads often become expensive in real-world applications. Techniques to reduce the memory footprint and computation precision for these models has been driven by the need to serve these models at scale, or run larger models locally on compute-limited resources. Quantization-aware training (QAT), has demonstrated the highest accuracy for most models; in QAT, precision reduction through quantization is included within the training loop, often requiring that the training pipeline and training data be accessed during the quantization process. Usually, QAT is incorporated within the fine-tuning phase (Yao et al., 2022), resulting in significant training overhead cost; these costs are particularly exacerbated for large-scale models. Post-training Quantization (PTQ), in contrast, quantizes existing pre-trained models, avoiding the need to retrain the model. The PTQ approach avoids many privacy hurdles associated with access to pre-training, enabling third parties to modify open-weight models and serve them efficiently on various hardware platforms (Lie, 2023; Frantar et al., 2022; Ashkboos et al., 2024).

However, while post-training quantization can reduce inference costs, reducing model precision is often associated with unintended consequences (Guha, 2024; Thangarasa, 2024). Research such as (Zhang et al., 2024) has shown that post-hoc quantization can have adverse effects on model alignment, and can be used to mitigate “unlearning” procedures that are applied to LLMs as copyright or safety filters. Quantization applied to multi-lingual LLMs have disparate effects on low-resource languages, particularly those that

use non-Latin scripts (Marchisio et al., 2024). These adverse affects also arise in QAT-trained models; even though final test accuracy is similar, performance of quantized LLMs can be significantly worse on complex tasks such as multi-turn dialog on standard benchmarks (Dutta et al., 2024).

Lossless Compression of LLM Weights Compared to the large body of work on lossy compression of LLM weights, there is relatively little work on lossless compression. An early paper (Han et al., 2015) proposed Huffman compression of convolutional neural network (CNN) weights, naively compressing entire 16-bit weights which incurs large performance overheads. For this reason, they do not actually implement Huffman coding, and instead only use run-length encoding (RLE) of sequences of zero weights. RLE is subsequently implemented in several other works, especially for CNNs that have sparse weight tensors (Chen et al., 2016). In contrast, HUFF-LLM proposes a lightweight hardware-friendly implementation of Huffman coding, integrates within systolic array and vector LLM accelerator architectures, demonstrating substantial performance and energy benefits.

Two recent works have addressed Huffman compression for LLMs: (Hershcovitch et al., 2024) propose to compress the exponent bits of weights via Huffman coding to reduce the cost of storing and downloading LLMs on cloud servers. For FP16 and BF16 models, they are able to achieve 17 - 33% compression with higher compression ratios coming from BF16 models due to the larger number of exponent bits. (Hao et al., 2024) use a similar approach by applying asymmetric numeral systems (ANS), an entropy coding method, to the exponent bits. In addition, they load the compressed weights to the GPU/TPU and thus achieve memory savings over (Hershcovitch et al., 2024) during inference. They are able to achieve 33% lossless compression on BF16 models, but also suffer a 33% inference slow down due to decompression.

Note that other lossless compression schemes exist. RLE, mentioned previously, exploits spatial correlations between inputs by encoding a sequence of identical weights as the weight value followed by the number of occurrences. LZW, a more sophisticated variant, exploits commonly occurring patterns in the input data (Welch, 1984). Both can be implemented synergistically after Huffman coding of individual weight values. We leave an evaluation of these methods as future work, but note that these incur additional hardware costs.

2.2. Hardware Accelerators for LLM Inference

Systolic Array Architectures The systolic array (SA) architecture, shown in Figure 1 consists of an array of processing elements (PEs) that perform multiply-and-accumulate

(MAC) operations, surrounded by on-chip buffers for data storage. Weights and activations are fetched from the weight buffer and activation buffer to the PEs, respectively. Data is streamed in from these buffers in a highly synchronized fashion such that each PE computes the dot product of a row of activations with a column of weights. However, it is crucial to maintain an uninterrupted data flow for correct performance of the systolic array, as any stalls or bubbles cause either incorrect computation or incur large performance penalties (Peltekis et al., 2023). This underscores the necessity of a Huffman decoder that operates without stalling the data stream (See Fig. 1). Note that the description above is for an "output stationary" (OS) systolic array. A slightly different architecture, referred to as weight stationary (WS) stores weights inside each PE and only streams in activations such that the output of each column produces a dot-product of a column of weights with activations.

Simba Vector Architectures To ensure the generality of our approach, we extended our evaluations to a parallel vector-processing optimized accelerator based on NVIDIA’s production-tested NVIDIA Deep Learning Accelerator (NVDLA) architecture (Sijstermans, 2018; Shao et al., 2019). The hardware model incorporates NVDLA dataflow-optimizations that reduce data-movement for transformers (Keller et al., 2022). Our evaluations use a single chiplet with an array of 16×16 Processing Elements (PEs) and a shared global buffer for activation storage (See Fig. 2). Each PE features dedicated local scratchpads for weights, inputs, and partial sums, along with vector multiply-accumulate (VMAC) units for parallel computation. The architecture is optimized for a 'local-weight-stationary' dataflow (where weights remain fixed in local memory to minimize data movement) (Venkatesan et al., 2019), operates at a nominal frequency of 2 GHz, and connects to external LPDDR4 DRAM via a 128 GB/s interface. For ease of reproducibility, detailed hardware specifications are provided in Table 3.

Lossless Compression in Hardware Prior work neural networks accelerators have applied lossless compression methods like RLE or sparse coding techniques, but have not implemented full end-to-end entropy coding methods like Huffman coding, in large measure due to its perceived costs. Prior work has implemented lossless compression tailored on CPUs for workloads relevant to general-purpose computing benchmarks. Bit-Plane Compression (BPC) (Kim et al., 2016), for example, introduces a novel compression algorithm to compress homogeneously typed memory blocks. BPC transforms the data and then applies run-length encoding and a frequent pattern encoding to compress the data. Buddy Compression (Choukse et al., 2020) uses BPC to connect GPU device memory to a "larger-but-slower buddy memory". Using a high-bandwidth interconnect between these two memories, they are able to send compressed data

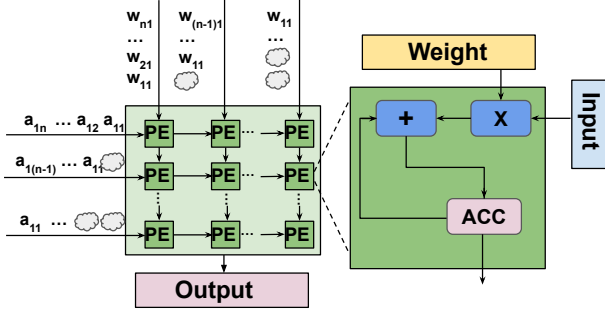


Figure 1. Systolic array diagram with a detailed look at the PE. Weights and activations are sent to the PEs at every clock cycle. Bubbles indicate delays which are necessary to maintain accuracy of the computations performed by the output stationary architecture. Colors are associated to different operands. Weights are yellow, inputs are light blue, and partial-sum/outputs are pink

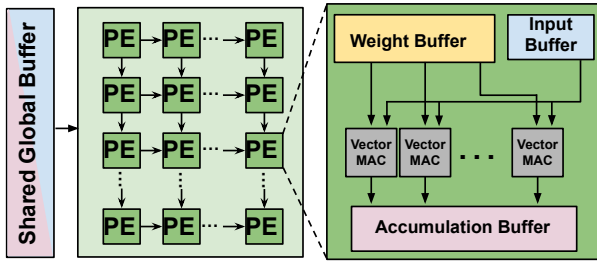


Figure 2. Simba-like architecture diagram with a detailed look at the PE. Colors are associated to different operands. Weights are yellow, inputs are light blue, and partial-sum/outputs are pink.

to the GPU memory while putting any data that doesn't fit on the GPU into the buddy memory. Selective Memory Compression (Nihaal & Mutyam, 2024) introduces a memory compression scheme that aims to reduce page thrashing by gradually compressing read-only pages.

3. The HUFF-LLM Scheme

3.1. Hardware-Friendly Huffman Compression

A key challenge with hardware implementations of Huffman decompression (and other entropy coding schemes) is that it is a variable length code. A naive hardware implementation of Huffman decompression can read a fixed number of codeword bits in each clock cycle, and output a decompressed source symbol when a match is found. Thus, when used to decompress a vector of weights, this scheme would output valid weights in some clock cycles and “bubbles” (indicating that absence of a valid weight) in others when no match is found. As noted in Section 2.2, neural network accel-

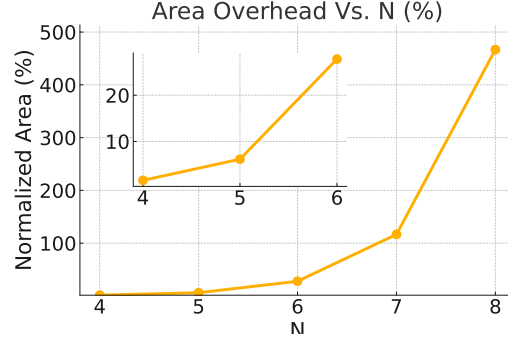


Figure 3. Area overhead of a CAM lookup for a single-cycle N-bit Huffman decoder normalized to a column of 128 FP16 multipliers, both clocked at 1 GHz. Area overheads of Huffman decoding grow quickly, leaving only $N=\{4,5\}$ as viable options.

Split	Entropy (Bits/Param)	Total Bits/Param
16	10.54	10.54
8-8	5.54, 5.03	10.57
1-5-5-5	1.00, 2.60, 4.97, 2.04	10.61
4-4-4-4	2.14, 3.91, 4.00, 1.34	11.09

Table 1. Entropy is calculated for each set of bits as defined by the split. Adding all entropy values together will give the average bits/parameter for the entire weight matrix.

erators like systolic arrays are carefully synchronized and require weights (and activations) to be output in each clock cycle for correct operation. Dealing with bubbles incurs a large performance penalty since the entire array needs to be stalled anytime a bubble is encountered, or requires complex control logic, extra buffering and a potential redesign of the accelerator logic.

On the other hand, a Huffman decoder that outputs a new weight value (or source symbol) in each clock cycle enables easy “plug-and-play” integration into existing neural network accelerators since the decoder can be added as an extra stage in the pipeline. Single cycle Huffman coding, however, introduces a new challenge: an input codeword must be matched against *all* possible 2^N codewords (assuming N -bit source symbols). In hardware, this logic is implemented using a content-addressable memory (CAM). However, CAMs have high hardware costs, and are typically limited to 32- or 64-entries in applications where single-cycle CAM look-ups are needed. Figure 3 plots the CAM overheads for 4 to 8 bit source symbols normalized to a column of 128 FP16 multipliers as reference (as we will see shortly, a single Huffman decoder will be shared across a column/row of MAC units). We see that overheads are 6% for $N=5$ bits, but balloon quickly for larger values of N .

Table 3.1 shows the entropy of Llama-3-8B FP16 weights is 10.54 bits/parameter; of course, as we have already ob-

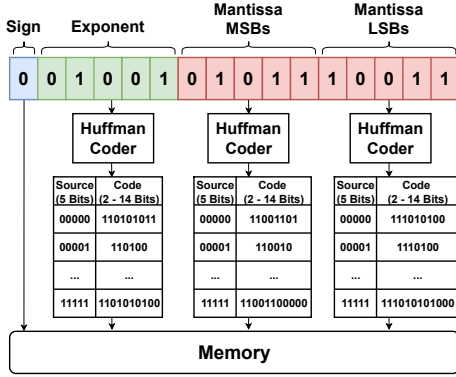


Figure 4. Our Huffman Compression method follows these steps for every parameter. It breaks a FP16 number into 4 groups of bits. The sign bit remains uncompressed. The exponent, and mantissa bits are sent through a Huffman Coder to be compressed. They are then stored in memory until they are needed for inference.

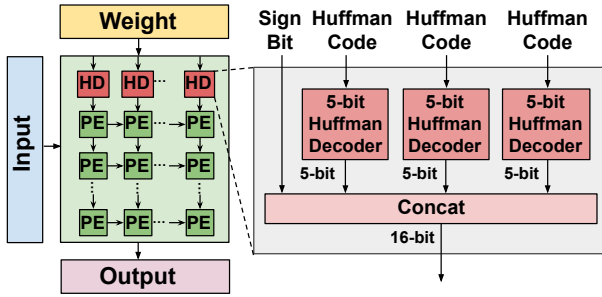


Figure 5. Systolic array and Huffman Decoder integration. served in Figure 3, N=16-bit Huffman decomposition is infeasible. Interestingly, we find that if, instead of Huffman compressing FP16 weights directly, we separately compress the 5-bit exponent, the 5 higher-order and 5 lower-order bits of the mantissa, the total entropy is only slightly larger at 10.61 bits/parameter. Note that in this scheme, we do not compress the sign bit. We refer to this as {1, 5, 5, 5} compression. Also shown in the table is the entropy for {8, 8} which also has a similar entropy of 10.57 bits/parameter, but is also infeasible from a hardware standpoint. Based on this analysis, we Huffman compress our weights using {1, 5, 5, 5} Huffman compression, as shown in Figure 4. Note that Huffman compression of LLM weights is performed only once and can be done offline on a CPU. Compressed weights are stored in memory, loaded into on-chip weight buffers in compressed format, and decompressed only when needed. Next, we describe our implementation of Huffman decomposition in our baseline hardware accelerators.

3.2. Hardware Integration of Huffman Decoders

Fig 5 shows how Huffman decoders are integrated within the baseline systolic array architecture described in Section 2.2. As noted previously, weights are streamed into the systolic

array from the weight buffer, one weight per clock cycle. In HUFF-LLM, weights are stored in the weight buffer in compressed form.

To enable computation, the Huffman-compressed weight data must be decoded before being fed into the systolic array. As depicted in Fig 5, a row of Huffman decompressors (HD) are inserted between the weight buffer’s output and the first row of processing elements (PEs) in the systolic array. Each HD module contains three 5-bit Huffman decoders. These decoders process the compressed data stream, decoding it into their respective parts of the 5-5-5 split decompressed data. To enable this, each column’s weight buffer is partitioned into three equally sized banks; each bank holds compressed weights from one of the three splits. The sign bit is passed through directly without modification. Finally, the sign bit, exponent, and mantissa bits are concatenated to reconstruct the 16-bit decompressed weight data.

Figure 7 shows the design of each 5-bit HD that enables it to output a decompressed weight in a single cycle. A 32-bit register holds compressed values fetched from the (compressed) weight buffer, along with a Start pointer (S) that points to the beginning of the current codeword. Assuming L_{max} is the number of bits in the longest codeword (note that L_{max} is known in advance, and $L_{max} < 32$ for any valid codebook), bits at positions S to $S + L_{max} - 1$ are used to match against all codewords stored in a 32-entry CAM. Each CAM entry also stores the 5-bit source symbol corresponding to each codeword and the codeword’s length, L . This source symbol is provided as an output from the decompressor and the start pointer is updated to $S \leftarrow S + L$. Finally, L bits are read from the weight buffer into the codeword register. In practice, a larger codeword register, say a 64-bit register can be used with the advantage that the weight buffer would only need to be accessed when fewer than 32 valid bits are left in the register.

We use the same HD design for the Simba-like vector architecture shown in Figure 2. The HD blocks are inserted between the distributed weight memory and vector MAC units. Since, as described, the HD blocks output a new decompressed weight per clock cycle without any bubbles or stalls, the throughput/performance of the accelerator is not impacted and no changes to the design are needed.

4. Experimental Setup

We now describe our experimental setup, including architectural parameters of our two baseline neural network accelerators, simulation methodology to estimate performance and energy with and without HUFF-LLM, LLMs and the datasets on which they are evaluated.

Tech node	16nm	
Systolic Array Size	128 × 128 PE	
PE Frequency	1GHz	
DRAM Bandwidth	64GB/s	128GB/s
Weight Buffer Size	16KB	
Activation Buffer Size	8KB	
Accumulator Buffer Size	4KB	
Dataflow	WS	OS

Table 2. Systolic Array Architecture Specifications.

Systolic array settings and simulation. Table 2 shows the architectural parameters of our baseline systolic array architecture, reflective of an edge tensor processing unit (TPU) similar to the Google Coral edge device (Suryavansh, 2020). The simulated architecture has a peak performance of 16 TOPs at 16b float precision, and was evaluated with 64 GBps and 128 GBps memory bandwidth. We model both output stationary (OS) and weight stationary (WS) architectures, as described in Section 2.2. We model the performance and energy of this architecture using a methodology similar to STAR-Sim (Sun et al., 2024) and SCALE-Sim (Samajdar et al., 2020) that are both widely used to model systolic array architectures. (more details in Appendix A.1). However, STAR-Sim and SCALE-Sim focus on modelling convolution operations while a majority of computations in LLMs are matrix multiplications (Wang et al., 2020). We modify SCALE-Sim for faster matrix multiplication simulations.

Simba architecture settings and simulation. We tabulate the architectural specifications of the evaluated Simba-like architecture in Table 3. Parameters were selected based on designs available in Nvidia Research’s Timeloop/Accelergy repository¹. The simulated architecture has a peak performance of 4 TOPs at 16b float precision, in-line with mobile NPUs (Jang et al., 2021), and was evaluated with 64 GBps and 128 GBps memory bandwidth, similar to the systolic array. Timeloop is an accelerator performance estimation tool developed by Nvidia (Parashar et al., 2019). Timeloop can model various scheduling strategies, and estimate how they impact the energy and latency of a computation. We use Timeloop’s hybrid search across all our experiments to minimize inference latency first and energy for mappings with the same latency. Energy costs are estimated via Accelergy via access counts generated from Timeloop. This approach is used to calculate energy for larger memories through Cacti (Balasubramonian et al., 2017) and smaller components such as address generators and register files using figures included in Aladdin (Shao et al., 2014).

¹<https://github.com/Accelergy-Project/timeloop-accelergy-exercises>

	Tech node	16nm	
Chip	PE Frequency	2GHz	
	Number of PEs	16	
	DRAM Bandwidth	64GB/s	128GB/s
	Weight Buffer Size	32KiB	
PE	Input Buffer Size	8KiB	
	Accumulator Buffer Size	3KiB	
	Number of Vector MACs	8	
	Vector MAC Width	8	

Table 3. Simba Architecture Specifications.

Benchmark	ArcEasy	MMLU	Winogrande
Avg Input Tokens	42	92	25
Standard Deviation	20	92	4

Table 4. Average input token length for benchmarks. Tokens are generated with Llama-3-8B’s tokenizer.

Benchmarks and Evaluated LLMs. Benchmarks such as MMLU (Hendrycks et al., 2020) are typically used to measure LLM capabilities. Works that focus on lossy compression (such as quantization) often use benchmark performance to show how much information was lost in the compression process. However, since HUFF-LLM is a lossless compression method, the compressed LLM maintains exactly the same accuracy as the original model by construction.

Alternatively, we can view LLM benchmarks from the perspective of their input context size. Different benchmarks have different average lengths of their inputs. For example, Arc-Easy (Clark et al., 2018) has an average length of approximately 42 input tokens, whereas MMLU has an average length of approximately 92 input tokens. Therefore, we use benchmarks to test how HUFF-LLM’s optimizations are impacted by various input token lengths.

Our performance estimation system uses the average token length of a benchmark query, rather than the actual benchmark questions. We report the average token length (as determined by the Llama-3-8B tokenizer) of each benchmark used in Table 4.

We perform compression tests and hardware simulations on various notable LLM families. We included the Llama (Dubey et al., 2024), OPT (Zhang et al., 2022), Qwen (Yang et al., 2024), and Vicuna (Chiang et al., 2023) model families to show how HUFF-LLM performs on different model architectures. In addition, we examine model sizes ranging from 3B to 13B parameters to see how model size impacts our compression scheme.

Model Name	FP16		BF16	
	Bits/Param	Ratio	Bits/Param	Ratio
Llama-3.2-3B	10.96	1.46	11.68	1.37
Llama-3-8B	10.96	1.46	11.68	1.37
Llama-2-13B	10.88	1.47	11.59	1.38
OPT-2.7B	13.68	1.17	11.68	1.37
OPT-6.7B	13.78	1.16	11.68	1.37
OPT-13B	13.68	1.17	11.59	1.38
Qwen-2.5-3B	10.96	1.46	11.68	1.37
Qwen-2.5-7B	10.96	1.46	11.68	1.37
Vicuna-7B	13.68	1.17	11.59	1.38
Vicuna-13B	13.68	1.17	11.59	1.38

Table 5. Compression ratio is calculated as an average of all weight matrices in each model. Bits/Param is calculated by dividing the uncompressed Bits/Param (16) by the compression ratio. Highest and lowest ratios are highlighted.

5. Experimental Results

5.1. Compression Experiments

We apply our Huffman compression method to FP16 variants of popular LLM families such as Llama, OPT, Qwen, and Vicuna. The total compression ratio is calculated by averaging the compression ratio of the attention and mlp weight matrices. These results can be found in Table 5.1. We notice that the Llama and Vicuna model families have similar compression ratios even at different model sizes. However, we also see that OPT and Vicuna have a notably smaller compression ratio. This suggests that there may be factors during the training stage that lead to certain distributions (and thus lossless compressibility) of the weights.

BF16 models are also very popular for inference. Therefore, we adapt our Huffman Compression method to work with BF16 models as well. We apply the same idea when splitting the bits. We find that the bits can be split 1-4-4-7. The seven mantissa bits at the end show little to no compressibility (in contrast to FP16). The sign bit remains uncompressed, and the exponent bits are split into two groups of four. We compress various models using our method and report the ratios in Table 5.1. We notice that all model families have a similar compression ratio in BF16. This is in contrast to FP16 where Vicuna and OPT had notably lower compression ratios. This could arise from the conversion process to BF16. We see that the compressibility of the mantissa (in FP16) has moved entirely to the exponent (in BF16). Therefore, in models where the FP16 compressibility is low (Vicuna), we are likely seeing higher compressibility in BF16 due to the larger number of exponent bits.

5.2. Hardware Results

Latency and Energy Savings Tables 6 and 7 present the latency and energy savings achieved when applying HUFF-

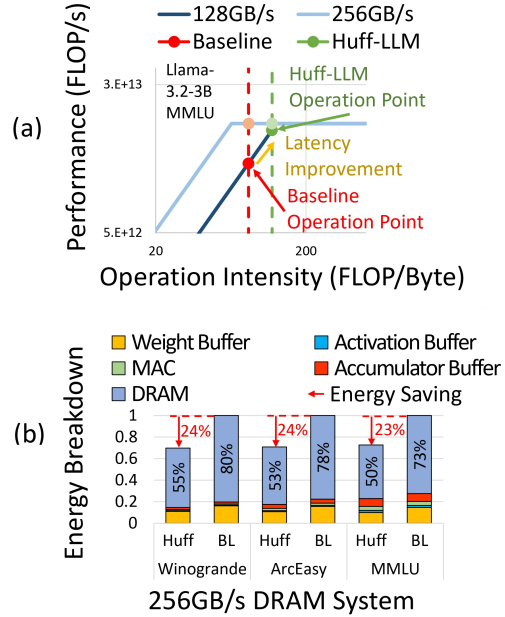


Figure 6. (a) Roofline plot of Systolic Arrays with 128GB/s and 256GB/s DRAM bandwidth. Dashed lines show the baseline and Huff-LLM models, with intersections marking operational points. (b) Energy breakdown of Huff-LLM and baseline model on the Systolic Array with 256GB/s DRAM bandwidth.

LLM to various FP16 models. We explore the Llama and OPT model families because they represent the best and worst case scenario for HUFF-LLM. Since compression ratio plays the largest role in determining these simulation results, we omit Qwen and Vicuna results due to their similarity with Llama and OPT respectively. In addition, full OPT results can be found in the Appendix in Section A.2.

The HUFF-LLM compression scheme leads to significant latency improvements, ranging from 26% to 31% for LLaMA models and 13% to 15% for OPT models. In terms of energy savings, LLaMA models also achieve notable gains of 16% to 26%, whereas OPT models see improvements of 3% to 10%. Additionally, reducing the DRAM bandwidth from 128 GB/s to 64 GB/s slightly enhances latency improvements by 2% to 3% but reduces energy savings by a similar margin. A comparable trend is observed for the OPT models. For Systolic Array architectures we see higher energy savings than for Simba architectures. This is due to the smaller weight buffer and increased reliance on DRAM access; the Systolic Array benefits more from HUFF-LLM because a larger portion of its overall energy consumption comes from memory-related operations.

The results thus far are for weight stationary (WS) architectures. Table 13 shows latency reductions and energy savings for output stationary (OS) systolic arrays; we observe Huff-LLM consistently achieves larger improvements in output stationary architectures because the output stationary system

Benchmark	Bandwidth	Llama 2-13B		Llama 3-8B		Llama 3.2-3B		OPT-13B	
		Systolic Array	Simba	Systolic Array	Simba	Systolic Array	Simba	Systolic Array	Simba
MMLU	64 GB/s	29.41%	28.18%	29.40%	31.33%	28.50%	31.07%	14.77%	14.05%
	128GB/s	27.17%	26.97%	28.97%	27.16%	28.22%	26.23%	14.01%	13.33%
Winogrande	64 GB/s	29.86%	31.11%	29.86%	31.11%	29.44%	31.38%	15.16%	14.29%
	128 GB/s	27.63%	29.60%	27.63%	29.58%	27.20%	29.58%	14.41%	13.33%
ArcEasy	64 GB/s	29.74%	31.40%	29.74%	31.35%	29.20%	31.33%	15.06%	14.29%
	128 GB/s	27.51%	29.60%	27.51%	29.58%	26.95%	29.53%	14.30%	13.33%

Table 6. Latency savings achieved when applying Huff-LLM to different FP16 models. Savings are simulated for Systolic Arrays and Simba with weight stationary (WS) architectures. Highest and lowest improvements are highlighted.

Benchmark	Bandwidth	Llama 2-13B		Llama 3-8B		Llama 3.2-3B		OPT-13B	
		Systolic Array	Simba	Systolic Array	Simba	Systolic Array	Simba	Systolic Array	Simba
MMLU	64 GB/s	23.76%	16.12%	23.75%	16.47%	22.78%	16.67%	9.14%	3.40%
	128GB/s	25.55%	19.79%	25.54%	19.33%	24.59%	19.72%	9.71%	6.41%
Winogrande	64 GB/s	24.25%	18.98%	24.25%	18.68%	23.80%	18.82%	9.56%	4.82%
	128 GB/s	26.03%	20.30%	26.02%	19.56%	25.58%	19.98%	10.13%	6.05%
ArcEasy	64 GB/s	24.12%	17.44%	24.12%	18.22%	23.53%	17.74%	9.45%	3.31%
	128 GB/s	25.90%	20.78%	25.90%	20.21%	25.32%	19.61%	10.02%	5.00%

Table 7. Energy savings achieved when applying Huff-LLM to various FP16 models. Savings are simulated for Systolic Arrays and Simba with weight stationary (WS) architectures. Highest and lowest improvements are highlighted.

has less weight reuse. This leads to higher weight movement overhead which can be reduced by Huff-LLM.

Area Overheads To estimate the area overheads of the proposed Huff-LLM scheme, we implemented a 5-bit Huffman Decoder and a systolic array PE in Verilog (a hardware description language) and synthesized these blocks for a Global Foundries 12nm (GF12) technology. Each PE has an area of $484\mu\text{m}^2$ while an HD with an empirically determined $L_{max} = 12$ is $1199.3\mu\text{m}^2$. For a 128×128 systolic array, the area overhead of Huff-LLMs is 6.13%. The area overhead at the full chip level would be even lower since we have not accounted for on-chip buffers in the denominator. Custom, highly-optimized CAM structures (Yue et al., 2024) can lower overheads further.

6. Discussion

Higher DRAM bandwidth diminishes the latency savings achieved by Huff-LLM, as weight movement accounts for a smaller fraction of the overall processing time. Additionally, as DRAM bandwidth increases, the system becomes more compute-bound. To evaluate the limits of Huff-LLM, we configure the Systolic Array with a DRAM bandwidth of 256GB/s and simulate its performance. To shed further light on Huff-LLM’s performance gains, Figure 6(a) presents a roofline plot (Williams et al., 2008) for Systolic Arrays executing the MMLU task on the Llama-3.2-3B model. Weight compression results in larger FLOPs/Byte since we need to fetch Bytes from memory, resulting in higher performance (FLOP/s) for 128 GB/s bandwidth. However for an

even higher 256 GB/s bandwidth, even the baseline model runs at peak performance, so compression will not reduce latency further (this is true for even 8-bit quantization). Despite the reduced latency improvement in higher bandwidth systems, Huff-LLM *still lowers energy consumption* by reducing memory access operations. Figure 6(b) illustrates the energy breakdown for Huff-LLM and the 16-bit baseline on the 256GB/s system, using the same MMLU task on the Llama-3.2-3B model. While system speed remains unchanged, Huff-LLM achieves a 24% reduction in energy consumption. This is largely because of the dominant energy costs of fetching data from memory, compared to other on-chip costs.

7. Conclusion

In this work, we propose Huff-LLM, an end-to-end model compression method for LLMs. We observe that Huffman Compression can be applied to subsets of weight parameters with minimal impact on the compression ratio. We use this observation to develop a compression scheme and hardware design that has minimal area overhead and is fast. We show up to 32% reduction in model size, up to 31% improvement in inference latency, and up to 26% reduction in energy cost.

Impact Statement

This paper presents work whose goal is to advance the field of Machine Learning. There are many potential societal consequences of our work, none which we feel must be specifically highlighted here.

References

- Ashkboos, S., Mohtashami, A., Croci, M. L., Li, B., Cameron, P., Jaggi, M., Alistarh, D., Hoefler, T., and Hensman, J. Quarot: Outlier-free 4-bit inference in rotated llms. *arXiv preprint arXiv:2404.00456*, 2024.
- Balasubramonian, R., Kahng, A. B., Muralimanohar, N., Shafiee, A., and Srinivas, V. Cacti 7: New tools for interconnect exploration in innovative off-chip memories. *ACM Transactions on Architecture and Code Optimization (TACO)*, 14(2):1–25, 2017.
- Chen, Y.-H., Krishna, T., Emer, J. S., and Sze, V. Eyeriss: An energy-efficient reconfigurable accelerator for deep convolutional neural networks. *IEEE journal of solid-state circuits*, 52(1):127–138, 2016.
- Chiang, W.-L., Li, Z., Lin, Z., Sheng, Y., Wu, Z., Zhang, H., Zheng, L., Zhuang, S., Zhuang, Y., Gonzalez, J. E., Stoica, I., and Xing, E. P. Vicuna: An open-source chatbot impressing gpt-4 with 90%* chatgpt quality, March 2023. URL <https://lmsys.org/blog/2023-03-30-vicuna/>.
- Choukse, E., Sullivan, M. B., O’Connor, M., Erez, M., Pool, J., Nellans, D., and Keckler, S. W. Buddy compression: Enabling larger memory for deep learning and hpc workloads on gpus. In *2020 ACM/IEEE 47th Annual International Symposium on Computer Architecture (ISCA)*, pp. 926–939. IEEE, 2020.
- Clark, P., Cowhey, I., Etzioni, O., Khot, T., Sabharwal, A., Schoenick, C., and Tafjord, O. Think you have solved question answering? try arc, the ai2 reasoning challenge. *arXiv preprint arXiv:1803.05457*, 2018.
- Dettmers, T., Lewis, M., Belkada, Y., and Zettlemoyer, L. Gpt3. int8 (): 8-bit matrix multiplication for transformers at scale. *Advances in Neural Information Processing Systems*, 35:30318–30332, 2022.
- Dubey, A., Jauhri, A., Pandey, A., Kadian, A., Al-Dahle, A., Letman, A., Mathur, A., Schelten, A., Yang, A., Fan, A., et al. The llama 3 herd of models. *arXiv preprint arXiv:2407.21783*, 2024.
- Dutta, A., Krishnan, S., Kwatra, N., and Ramjee, R. Accuracy is not all you need. *arXiv preprint arXiv:2407.09141*, 2024.
- Frantar, E., Ashkboos, S., Hoefler, T., and Alistarh, D. Gptq: Accurate post-training quantization for generative pre-trained transformers. *arXiv preprint arXiv:2210.17323*, 2022.
- Guha, E. Does reduced precision hurt? Blog post, 2024. URL <https://sambanova.ai/blog/does-reduced-precision-hurt>. Accessed: February 4, 2025.
- Han, S., Mao, H., and Dally, W. J. Deep compression: Compressing deep neural networks with pruning, trained quantization and Huffman coding. *arXiv preprint arXiv:1510.00149*, 2015.
- Hao, Y., Cao, Y., and Mou, L. Neuzip: Memory-efficient training and inference with dynamic compression of neural networks. *arXiv preprint arXiv:2410.20650*, 2024.
- Hendrycks, D., Burns, C., Basart, S., Zou, A., Mazeika, M., Song, D., and Steinhardt, J. Measuring massive multitask language understanding. *arXiv preprint arXiv:2009.03300*, 2020.
- Hershcovitch, M., Wood, A., Choshen, L., Girmonsky, G., Leibovitz, R., Ennmouri, I., Malka, M., Chin, P., Sundararaman, S., and Harnik, D. Zipnn: Lossless compression for ai models. *arXiv preprint arXiv:2411.05239*, 2024.
- Hong, J., Duan, J., Zhang, C., Li, Z., Xie, C., Lieberman, K., Diffenderfer, J., Bartoldson, B., Jaiswal, A., Xu, K., et al. Decoding compressed trust: Scrutinizing the trustworthiness of efficient llms under compression. *arXiv preprint arXiv:2403.15447*, 2024.
- Jang, J.-W., Lee, S., Kim, D., Park, H., Ardestani, A. S., Choi, Y., Kim, C., Kim, Y., Yu, H., Abdel-Aziz, H., Park, J.-S., Lee, H., Lee, D., Kim, M. W., Jung, H., Nam, H., Lim, D., Lee, S., Song, J.-H., Kwon, S., Hassoun, J., Lim, S., and Choi, C. Sparsity-aware and reconfigurable npu architecture for samsung flagship mobile soc. In *Proceedings of the 48th Annual International Symposium on Computer Architecture, ISCA ’21*, pp. 15–28. IEEE Press, 2021. ISBN 9781450390866. doi: 10.1109/ISCA52012.2021.00011. URL <https://doi.org/10.1109/ISCA52012.2021.00011>.
- Keller, B., Venkatesan, R., Dai, S., Tell, S. G., Zimmer, B., Dally, W. J., Thomas Gray, C., and Khailany, B. A 17–95.6 tops/w deep learning inference accelerator with per-vector scaled 4-bit quantization for transformers in 5nm. In *2022 IEEE Symposium on VLSI Technology and Circuits (VLSI Technology and Circuits)*, pp. 16–17, 2022. doi: 10.1109/VLSITechnologyandCir46769.2022.9830277.
- Kim, J., Sullivan, M., Choukse, E., and Erez, M. Bit-plane compression: Transforming data for better compression in many-core architectures. *ACM SIGARCH Computer Architecture News*, 44(3):329–340, 2016.
- Lie, S. Cerebras architecture deep dive: First look inside the hardware/software co-design for deep learning. *IEEE Micro*, 43(3):18–30, 2023.

- Lin, J., Tang, J., Tang, H., Yang, S., Chen, W.-M., Wang, W.-C., Xiao, G., Dang, X., Gan, C., and Han, S. Awq: Activation-aware weight quantization for on-device llm compression and acceleration. *Proceedings of Machine Learning and Systems*, 6:87–100, 2024.
- Marchisio, K., Dash, S., Chen, H., Aumiller, D., Üstün, A., Hooker, S., and Ruder, S. How does quantization affect multilingual llms? *arXiv preprint arXiv:2407.03211*, 2024.
- Nihaal, A. and Mutyam, M. Selective memory compression for gpu memory oversubscription management. In *Proceedings of the 53rd International Conference on Parallel Processing*, pp. 189–198, 2024.
- Parashar, A., Raina, P., Shao, Y. S., Chen, Y.-H., Ying, V. A., Mukkara, A., Venkatesan, R., Khailany, B., Keckler, S. W., and Emer, J. Timeloop: A systematic approach to dnn accelerator evaluation. In *2019 IEEE International Symposium on Performance Analysis of Systems and Software (ISPASS)*, pp. 304–315, 2019. doi: 10.1109/ISPASS.2019.00042.
- Peltekis, C., Filippas, D., Dimitrakopoulos, G., Nicopoulos, C., and Pnevmatikatos, D. Arrayflex: A systolic array architecture with configurable transparent pipelining. In *2023 Design, Automation and Test in Europe Conference and Exhibition (DATE)*, pp. 1–6, 2023. doi: 10.23919/DATE56975.2023.10136913.
- Samajdar, A., Joseph, J. M., Zhu, Y., Whatmough, P., Mattina, M., and Krishna, T. A systematic methodology for characterizing scalability of dnn accelerators using scale-sim. In *2020 IEEE International Symposium on Performance Analysis of Systems and Software (ISPASS)*, pp. 58–68, 2020. doi: 10.1109/ISPASS48437.2020.00016.
- Shao, Y. S., Reagen, B., Wei, G.-Y., and Brooks, D. Aladdin: A pre-rtl, power-performance accelerator simulator enabling large design space exploration of customized architectures. In *Proceeding of the 41st Annual International Symposium on Computer Architecture, ISCA '14*, pp. 97–108. IEEE Press, 2014. ISBN 9781479943944.
- Shao, Y. S., Clemons, J., Venkatesan, R., Zimmer, B., Fojtik, M., Jiang, N., Keller, B., Klinefelter, A., Pinckney, N., Raina, P., Tell, S. G., Zhang, Y., Dally, W. J., Emer, J., Gray, C. T., Khailany, B., and Keckler, S. W. Simba: Scaling deep-learning inference with multi-chip-module-based architecture. In *Proceedings of the 52nd Annual IEEE/ACM International Symposium on Microarchitecture, MICRO '52*, pp. 14–27, New York, NY, USA, 2019. Association for Computing Machinery. ISBN 9781450369381. doi: 10.1145/3352460.3358302. URL <https://doi.org/10.1145/3352460.3358302>.
- Sijstermans, F. The nvidia deep learning accelerator. In *Hot Chips*, volume 30, pp. 19–21, 2018.
- Sun, X., Peng, X., Zhang, S. Q., Gomez, J., Khwa, W.-S., Sarwar, S. S., Li, Z., Cao, W., Wang, Z., Liu, C., Chang, M.-F., De Salvo, B., Akarvardar, K., and Wong, H.-S. P. Estimating power, performance, and area for on-sensor deployment of ar/vr workloads using an analytical framework. *ACM Trans. Des. Autom. Electron. Syst.*, 29(6), September 2024. ISSN 1084-4309. doi: 10.1145/3670404. URL <https://doi.org/10.1145/3670404>.
- Suryavansh, M. Google coral edge tpu board vs nvidia jetson nano dev board hardware comparison, 2020.
- Thangarasa, V. Llama3.1 model quality evaluation: Cerebras, groq, sambanova, together, and fireworks. Blog post, 2024. URL <https://cerebras.ai/blog/>. Accessed: February 4, 2025.
- Venkatesan, R., Shao, Y. S., Wang, M., Clemons, J., Dai, S., Fojtik, M., Keller, B., Klinefelter, A., Pinckney, N., Raina, P., Zhang, Y., Zimmer, B., Dally, W. J., Emer, J., Keckler, S. W., and Khailany, B. Magnet: A modular accelerator generator for neural networks. In *2019 IEEE/ACM International Conference on Computer-Aided Design (ICCAD)*, pp. 1–8, 2019. doi: 10.1109/ICCAD45719.2019.8942127.
- Wang, H., Zhang, Z., and Han, S. Spatten: Efficient sparse attention architecture with cascade token and head pruning. *2021 IEEE International Symposium on High-Performance Computer Architecture (HPCA)*, pp. 97–110, 2020. URL <https://api.semanticscholar.org/CorpusID:229298088>.
- Welch, T. A. A technique for high-performance data compression. *Computer*, 17(06):8–19, 1984.
- Williams, S., Patterson, D., Oliker, L., Shalf, J., and Yelick, K. The roofline model: A pedagogical tool for program analysis and optimization. In *2008 IEEE Hot Chips 20 Symposium (HCS)*, pp. 1–71, 2008. doi: 10.1109/HOTCHIPS.2008.7476531.
- Xu, Z., Gupta, A., Li, T., Bentham, O., and Srikumar, V. Beyond perplexity: Multi-dimensional safety evaluation of llm compression. *arXiv preprint arXiv:2407.04965*, 2024.
- Yang, A., Yang, B., Zhang, B., Hui, B., Zheng, B., Yu, B., Li, C., Liu, D., Huang, F., Wei, H., et al. Qwen2.5 technical report. *arXiv preprint arXiv:2412.15115*, 2024.

Yao, Z., Yazdani Aminabadi, R., Zhang, M., Wu, X., Li, C., and He, Y. Zeroquant: Efficient and affordable post-training quantization for large-scale transformers. *Advances in Neural Information Processing Systems*, 35: 27168–27183, 2022.

Yue, Z., Xiang, X., Tu, F., Wang, Y., Wang, Y., Wei, S., Hu, Y., and Yin, S. 15.1 a 0.795 fJ/bit physically-unclonable function-protected tcam for a software-defined networking switch. In *2024 IEEE International Solid-State Circuits Conference (ISSCC)*, volume 67, pp. 276–278. IEEE, 2024.

Zhang, S., Roller, S., Goyal, N., Artetxe, M., Chen, M., Chen, S., Dewan, C., Diab, M., Li, X., Lin, X. V., et al. Opt: Open pre-trained transformer language models. *arXiv preprint arXiv:2205.01068*, 2022.

Zhang, Z., Wang, F., Li, X., Wu, Z., Tang, X., Liu, H., He, Q., Yin, W., and Wang, S. Does your llm truly unlearn? an embarrassingly simple approach to recover unlearned knowledge. *arXiv preprint arXiv:2410.16454*, 2024.

A. Additional results

You can have as much text here as you want. The main body must be at most 8 pages long. For the final version, one more page can be added. If you want, you can use an appendix like this one.

The `\onecolumn` command above can be kept in place if you prefer a one-column appendix, or can be removed if you prefer a two-column appendix. Apart from this possible change, the style (font size, spacing, margins, page numbering, etc.) should be kept the same as the main body.

A.1. Analytical Simulator

To map the multiplication of input matrix I and weight matrix W , with shape of $I_H \times I_W$ and $W_H \times W_W$, we adopted same dataflow-dependent mapping schemes as SCALE-Sim (Samajdar et al., 2020), where the dimensions of two operand matrices are defined as $S_R \times T$ and $T \times S_C$, as shown in Figure 5. S_R and S_C are the specific workload dimensions mapped to the rows and columns of a systolic array, respectively, and T is the temporal dimension, along which the data are being streamed into the systolic array. Table A.1 summarizes the definition of S_R , S_C , and T depending on the dataflow configuration.

Dataflow	S_R	S_C	T
Weight Stationary	W_H	W_W	I_H
Output Stationary	I_H	W_W	W_H

Table 8. Spatial and temporal mapping of the input matrix (I) with shape of $I_H \times I_W$ and weight matrix (W) with shape of $W_H \times W_W$ to the rows and columns of a systolic array. I_W is equal to W_H .

Since one systolic array may not be sufficient to accommodate the entire matrix computation in common LLM layers, the workload is typically partitioned into "folds" (Samajdar et al., 2020) with respect to the rows (R) and columns (C) of the PE array. The number of folds along the row dimension (F_R) and column dimension (F_C) can be calculated as:

$$F_R = \lceil \frac{S_R}{R} \rceil, F_C = \lceil \frac{S_C}{C} \rceil \quad (2)$$

We use the same principle as SCALE-Sim (Samajdar et al., 2020) to model the number of compute cycles as below:

$$L_{COMP} = (2R + C + T - 2) \cdot F_R \cdot F_C \quad (3)$$

For modeling of buffer access, we consider the stationary data and streaming data separately. The stationary operand in the systolic array will get updated only after being fully reused by the streaming operand, so the number of read accesses of stationary data is equal to the number of stationary data. In contrast, the streaming data may need to be reloaded by multiple times, for which the reloading count is equal to the number of folds. As such, the number of weight buffer read accesses (WB_{RD}) and the number of input buffer read accesses (IB_{RD}) can be modeled as below:

$$WB_{RD} = \begin{cases} W_H \cdot W_W, & \text{if } WS \\ W_W \cdot W_H \cdot \lceil \frac{I_H}{R} \rceil, & \text{if } OS \end{cases} \quad (4)$$

$$IB_{RD} = \begin{cases} W_H \cdot I_H \cdot \lceil \frac{W_W}{C} \rceil, & \text{if } WS \\ I_H \cdot W_H \cdot \lceil \frac{W_W}{C} \rceil, & \text{if } OS \end{cases} \quad (5)$$

The MAC latency is modeled as the product of the total compute cycles and the cycle time. The memory read/write latency is modeled as the division of read/write data and buffer bandwidth.

The MAC energy is modeled as the product of the total number of MAC operations and the energy per MAC operation. The memory read/write access energy is modeled as the product of the unit energy per read/write access and the number of read/write accesses.

A.2. Additional Results

Full OPT results and output stationary results are included in this section.

Benchmark	Bandwidth	OPT-13B	OPT-6.7B	OPT-2.7B
MMLU	64 GB/s	14.77%	14.63%	14.23%
	128 GB/s	14.01%	13.87%	13.47%
Winogrande	64 GB/s	15.16%	15.10%	14.93%
	128 GB/s	14.41%	14.35%	14.17%
ArcEasy	64 GB/s	15.06%	14.98%	14.75%
	128 GB/s	14.30%	14.22%	13.99%

Table 9. Latency saving when compressing the OPT model weights from 16-bit to 14-bit. The results are from the Star system simulation.

Benchmark	Bandwidth	OPT-13B	OPT-6.7B	OPT-2.7B
MMLU	64 GB/s	9.14%	9.00%	8.57%
	128 GB/s	9.71%	9.57%	9.14%
Winogrande	64 GB/s	9.56%	9.50%	9.31%
	128 GB/s	10.13%	10.06%	9.88%
ArcEasy	64 GB/s	9.45%	9.37%	9.12%
	128 GB/s	10.02%	9.94%	9.69%

Table 10. Energy saving when compressing the OPT model weights from 16-bit to 14-bit. The results are from the Star system simulation.

Benchmark	Bandwidth	OPT-13B	OPT-6.7B	OPT-2.7B
MMLU	64 GB/s	14.05%	14.29%	14.05%
	128 GB/s	13.33%	13.35%	13.33%
Arceasy	64 GB/s	14.29%	14.2%	14.4%
	128 GB/s	13.33%	13.29%	13.36%
Winogrande	64 GB/s	14.29%	14.35%	14.31%
	128 GB/s	13.33%	13.35%	13.33%

Table 11. Latency saving for different benchmarks at 64 GB/s and 128 GB/s bandwidth simulated on timeloop on Simba for OPT models with compressed weights from 16-bit to 14-bit.

Benchmark	Bandwidth	OPT-13B	OPT-6.7B	OPT-2.7B
MMLU	64 GB/s	3.4%	3.5%	3.38%
	128 GB/s	6.41%	6.93%	6.89%
Arceasy	64 GB/s	3.31%	3.48%	4.02%
	128 GB/s	5%	5.78%	6.1%
Winogrande	64 GB/s	4.82%	5.13%	5.2%
	128 GB/s	6.05%	6.23%	6.37%

Table 12. Energy saving for different benchmarks at 64 GB/s and 128 GB/s bandwidth simulated on timeloop on Simba for OPT models with compressed weights from 16-bit to 14-bit.

Benchmark	Bandwidth	Llama 2-13B		Llama 3-8B		Llama 3.2-3B	
		Latency	Energy	Latency	Energy	Latency	Energy
MMLU	64 GB/s	31.00%	24.37%	30.99%	24.36%	30.11%	23.39%
	128GB/s	28.31%	26.69%	28.30%	26.68%	27.38%	25.75%
Winogrande	64 GB/s	31.44%	24.85%	31.44%	24.85%	31.03%	24.40%
	128 GB/s	28.76%	27.16%	28.76%	27.16%	28.34%	26.73%
ArcEasy	64 GB/s	31.33%	24.73%	31.32%	24.72%	30.79%	24.14%
	128 GB/s	28.65%	27.04%	28.64%	27.04%	28.09%	26.47%

Table 13. Latency and Energy savings achieved when applying Huff-LLM FP16 models. Simulations are performed on an output stationary (OS) systolic array architecture.

A.3. Huffman Decoder Figure

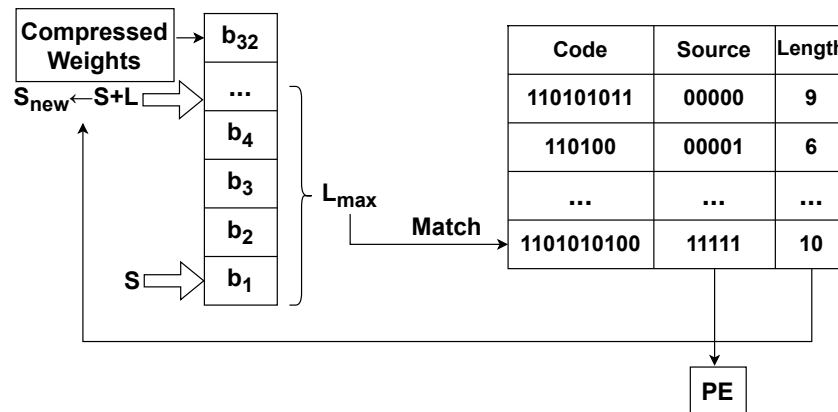


Figure 7. Each Huffman Decoder module follows the process shown in this figure. L_{max} bits are taken from the register and a match is found in the Huffman Table. Afterwards, the decoded source symbol is sent to the PE while the length is sent to update the start position S .